Original Research Article

GREENHOUSE GASES SCIENCE AND TECHNOLOGY

Hierarchical calibration and validation framework of bench-scale computational fluid dynamics simulations for solvent-based carbon capture. Part 2: Chemical absorption across a wetted wall column

Chao Wang, **Zhijie Xu and Kevin Lai**, Pacific Northwest National Laboratory, Physical and Computational Sciences Directorate, Richland, WA
Greg Whyatt, Energy and Environment Directorate, Pacific Northwest National Laboratory, Richland, WA
Peter W. Marcy, Los Alamos National Laboratory, Statistical Sciences Group, Los Alamos, NM
Xin Sun, Oak Ridge National Laboratory, Energy and Transportation Science Division, Oak Ridge, TN

Abstract: Part 1 of this paper presents a numerical model for non-reactive physical mass transfer across a wetted wall column (WWC). In Part 2, we improved the existing computational fluid dynamics (CFD) model to simulate chemical absorption occurring in a WWC as a bench-scale study of solvent-based carbon dioxide (CO_2) capture. To generate data for WWC model validation, CO_2 mass transfer across a monoethanolamine (MEA) solvent was first measured on a WWC experimental apparatus. The numerical model developed in this work can account for both chemical absorption and desorption of CO_2 in MEA. In addition, the overall mass transfer coefficient predicted using traditional/empirical correlations is conducted and compared with CFD prediction results for both steady and wavy falling films. A Bayesian statistical calibration algorithm is adopted to calibrate the reaction rate constants in chemical absorption/desorption of CO_2 across a falling film of MEA. The posterior distributions of the two transport properties, i.e., Henry's constant and gas diffusivity in the non-reacting nitrous oxide (N_2O)/MEA system obtained from Part 1 of this study, serves as priors for the calibration of CO_2 reaction rate constants after using the N_2O/CO_2 analogy method. The calibrated model can be used to predict the CO_2 mass transfer in a WWC for a wider range of operating conditions.

Keywords: computational fluid dynamics; carbon capture; chemical absorption; Bayesian calibration; wetted wall column; hierarchical calibration and validation

Correspondence to: Chao Wang, Physical and Computational Sciences Directorate, Pacific Northwest National Laboratory, 902 Battelle Boulevard, P.O. Box 999, MSIN K7-90, Richland, WA 99352, USA.
E-mail: chao.wang@pnnl.gov
Received June 15, 2017; revised August 22, 2017; accepted August 25, 2017
Published online at Wiley Online Library (wileyonlinelibrary.com). DOI: 10.1002/ghg.1727

Introduction

Much research has been devoted to developing carbon capture technology including amine-based solid sorbent capture,[1–4] impact of rivulet flow on mass transfer rate,[5,6] etc. The purpose of this paper is to present a validation and calibration framework for predicting chemical absorption of carbon dioxide (CO_2) across a monoethanolamine (MEA) solution. Thus, a comprehensive understanding of the reaction kinetics between CO_2 and amine is essential in getting precise information about the chemical reaction rates,[7–9] as well as detailed knowledge of the reaction mechanism.[10–15] Hikita *et al.*[16] used a rapid-mixing thermal method to show that reactions between CO_2 and MEA in aqueous solution appeared to be first-order in the amine concentration. Their results were reproduced and confirmed by Laddha and Danckwerts,[17] who absorbed CO_2 in a stirred cell into aqueous solutions of MEA. The computational model developed in this work adopts this finding to represent the chemical reaction rates between CO_2 and MEA. Next, the reaction mechanisms of CO_2 absorption by MEA are normally described using three sub-reactions to indicate vital influence on the CO_2/MEA reaction,[18] which include:

Carbamate formation:

$$CO_2 + 2RNH_2 \rightarrow RNHCOO^- + RNH_3^+,$$

Bicarbonate formation:

$$CO_2 + RNH_2 + H_2O \rightarrow HCO_3^- + RNH_3^+,$$

Carbamate reversion:

$$RNHCOO^- + CO_2 + 2H_2O \rightarrow HCO_3^- + 2RNH_3^+,$$

where $R = CH_2CH_2OH$. Astarita *et al.*[19] suggest that the rate of bicarbonate formation is negligible because of MEA carbamate's high stability. In addition, the overall absorption rate can be approximated as irreversible, making the carbamate reversion insignificant. As a result, the overall CO_2/MEA reaction rate is dominated by the carbamate formation.

The mass transfer between CO_2 and MEA also includes physical absorption, which is mainly dominated by CO_2 solubility/diffusivity in MEA solution.[20–27] Because of the chemical reactions between CO_2 and MEA, the physical solubility/diffusivity of CO_2 in MEA solution cannot be directly measured. However, the estimation of solubility/diffusivity can be made using the nitrous oxide (N_2O) analogy method,[28] which states that the ratio of solubility/diffusivity of N_2O/CO_2 in MEA solution is the same as that in water. This analogy is made based on the similarities in mass and molecular structure between CO_2 and N_2O. The solubility/diffusivity in the non-reacting N_2O/MEA system is obtained in Part 1 of this study.[29]

In the present work, the absorption accompanied by chemical reactions occurring in a wetted wall column (WWC) is investigated using numerical simulation, conventional/empirical correlations, and experimental measurements. Moreover, we aim to provide a computational fluid dynamics (CFD) mechanism-based predictive framework that includes using statistical methods to determine the confidence bounds for the overall mass transfer coefficient under various operating conditions of a WWC for the reactive CO_2/MEA system. The remainder of the paper is organized as follows. The next section describes the experimental study of reactive CO_2 absorption into a falling film of MEA in a WWC and is followed by a description of the numerical modeling. Then the CFD simulation and conventional/empirical correlation results are discussed before we provide the model calibration analyses.

Experimental study of the CO_2/MEA system

For a CO_2/MEA system, the experiments are conducted using the same experimental apparatus introduced in Part 1 of this work,[29] except the gas being transported is CO_2 instead of N_2O. The mass transfer coefficient K_G (mol/(Pa·s·m^8)) for a CO_2/MEA system can be calculated by Eqn (1):

$$K_G = \frac{J}{\Delta P}, \tag{1}$$

where J denotes the mass transfer flux at the gas-liquid interface and ΔP is the log mean driving force defined as

$$\Delta P = \frac{\left(P_{CO_2,in} - P^*_{CO_2}\right) - \left(P_{CO_2,out} - P^*_{CO_2}\right)}{ln\left[\frac{P_{CO_2,in} - P^*_{CO_2}}{P_{CO_2,out} - P^*_{CO_2}}\right]}, \tag{2}$$

where $P^*_{CO_2}$ is the equilibrium CO_2 pressure. If CO_2 loading exceeds 0.4 (mol CO_2/mol MEA), $P^*_{CO_2}$ may vary significantly for a small change in CO_2 loading as shown in Fig. 1.[30] Therefore, the $P^*_{CO_2}$ measurement is

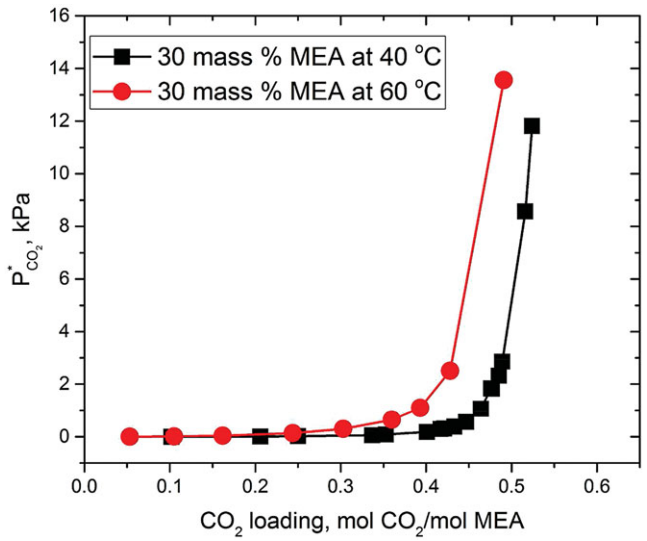

Figure 1. $P^*_{CO_2}$ versus CO_2 loading. $P^*_{CO_2}$ may vary significantly for a small change in loading if CO_2 loading exceeds 0.4. The data in this plot are obtained from Aronu *et al.*[30]

important for determining the log mean driving force, especially for high CO_2 loading solvent.

Table 1 presents the data for CO_2-related measurements. Mass transfer is measured on the WWC while operating under various conditions. The varied parameters include MEA mass fraction, CO_2 loading, solvent flow rate, gas flow rate, CO_2 molar fraction, and temperature. These diverse parameters are shown in Table 1, columns 2–7. In column 8, the $P^*_{CO_2}$ used in calculating the driving force is provided. Column 9 shows the experimental measurement of CO_2 flux, while column 10 shows the calculated overall mass transfer coefficient, K_G. For solution loadings and temperatures expected to produce a $P^*_{CO_2}$ of less than 1.5% of the inlet gas CO_2 partial pressure, the $P^*_{CO_2}$ value is treated as zero. This could result in a small overestimate of the driving force, which would bias the overall mass transfer coefficient low by up to 1.5%. However, this level of error was deemed to be within our experimental accuracy. If the $P^*_{CO_2}$ is expected to be more than 1.5% of the inlet gas CO_2 partial pressure, the $P^*_{CO_2}$ of the solution is estimated by measuring flux at two additional inlet CO_2 concentrations. The results are plotted to estimate the CO_2 pressure providing zero flux. More specifically, after three measurement points are taken, a flux versus pressure plot is drawn, and the x-axis intercept of a linear fit of these three points is used to estimate $P^*_{CO_2}$. Figure 2 shows how the P^* is approximated for test run No. 6. The P^* has been estimated this way for runs No. 6–8, 13–15, 20, 21, 28, 29, and 32.

Numerical modeling of WWC

Governing equations

A volume of fluid (VOF) model together with mass and momentum conservation equations are employed and have been introduced in Part 1 of this work, aiming to solve for the hydrodynamics of two Newtonian, incompressible, isothermal, and immiscible fluid flows. The one-fluid equation[31,32] considering advection, diffusion, interface mass transport, and chemical reactions is implemented to calculate gas concentration in both phases by using only one equation for the entire domain:

$$\frac{\partial c_i}{\partial t} + \nabla \cdot (\boldsymbol{u} c_i - \mathrm{D}_i \nabla c_i - \Gamma_i) - W_i = 0, \qquad (3)$$

where

$$\Gamma_i = -\mathrm{D}_i \frac{c_i (1 - k_i)}{\alpha_L + k_i (1 - \alpha_L)} \nabla \alpha_L,$$

$$D_i = \frac{D_{i,L} D_{i.g}}{\alpha_L D_{i,g} + (1 - \alpha_L) D_{i,L}}.$$

Here, c_i represents the concentration for species i; t is time; $\boldsymbol{u}$ is velocity; D_i is diffusivity which is computed by the harmonic interpolation; $k_i = c^I_{i,g}/c^I_{i,L}$ denotes the dimensionless Henry's constant, where $c^I_{i,g}$ and $c^I_{i,L}$ are the gas phase and liquid phase concentration of species i at the gas-liquid interface; and α_L is the volume fraction of the liquid phase. The term Γ in Eqn (3) accounts for discontinuity at the gas-liquid interface. The last term, W_i, is the production term, which relates to the chemical reaction.

When the chemical equilibrium state is reached in the liquid phase, the chemical equilibrium reaction and equilibrium constant of the carbamate formation can be written as

$$RNHCOO^- + RNH_3^+ \overset{K'_{CO_2}}{\Leftrightarrow} CO_2\,(aq) + 2RNH_2$$

$$K'_{CO_2} = \frac{[RNH_2]^2 \left[CO_2\,(aq)\right]}{\left[RNH_3^+\right] [RNHCOO^-]}, \qquad (4)$$

where $CO_2(aq)$ denotes the physically absorbed CO_2 in aqueous solution of MEA and K'_{CO_2} is the chemical equilibrium constant for the CO_2 absorption reaction. The molar fraction of MEA and the products (or reactants) can be introduced as

Table 1. CO_2/MEA experimental data.

Run#	MEA mass fraction	CO_2 loading (mol CO_2/mol MEA)	Solvent flow rate, cc/min	Gas flow rate, sccm	CO_2 molar fraction	Temp. °C	P*, Pa	CO_2 flux, mol/(m^2 s)	K_G, mol/(Pa · s · m^2)
1	0.25	0.30	450	4000	0.115	42	0	1.30E-02	1.32E-06
2	0.10	0.10	495	4344	0.070	45	0	9.17E-03	1.57E-06
3	0.10	0.20	590	2126	0.191	27	0	1.47E-02	8.64E-07
4	0.10	0.20	352	2724	0.086	49	0	7.71E-03	1.11E-06
5	0.10	0.30	550	2558	0.164	55	0	1.13E-02	8.69E-07
6	0.10	0.40	318	2284	0.183	47	1.18E+03	8.71E-03	6.04E-07
7	0.10	0.40	404	3474	0.158	59	6.14E+03	4.46E-03	6.94E-07
8	0.10	0.50	558	2681	0.056	32	1.39E+03	1.10E-03	2.95E-07
9	0.20	0.10	322	2342	0.032	30	0	3.19E-03	1.27E-06
10	0.20	0.20	426	3735	0.142	31	0	1.65E-02	1.32E-06
11	0.20	0.20	466	3899	0.064	38	0	7.69E-03	1.43E-06
12	0.20	0.30	338	5549	0.134	53	0	1.43E-02	1.29E-06
13	0.20	0.40	410	3345	0.127	43	7.24E+02	7.37E-03	7.06E-07
14	0.20	0.40	475	3635	0.043	56	3.09E+03	3.86E-04	8.74E-07
15	0.20	0.50	521	2861	0.147	39	2.45E+03	3.92E-03	3.56E-07
16	0.30	0.10	363	4682	0.106	41	0	1.85E-02	2.08E-06
17	0.30	0.20	532	5130	0.175	33	0	2.41E-02	1.53E-06
18	0.30	0.20	375	5241	0.049	56	0	7.77E-03	2.04E-06
19	0.30	0.30	488	3107	0.110	52	0	1.16E-02	1.33E-06
20	0.30	0.40	432	4189	0.102	41	−8.20E+00	7.40E-03	8.17E-07
21	0.30	0.40	458	4839	0.079	51	1.17E+03	5.34E-03	9.64E-07
22	0.30	0.50	308	5991	0.196	25	0	5.04E-03	2.65E-07
23	0.40	0.10	537	4431	0.116	46	0	2.33E-02	2.49E-06
24	0.40	0.20	513	4066	0.121	36	0	1.69E-02	1.61E-06
25	0.40	0.20	570	5673	0.179	59	0	3.31E-02	2.36E-06
26	0.40	0.30	378	5301	0.040	34	0	4.02E-03	1.13E-06
27	0.40	0.40	588	5790	0.093	28	0	6.44E-03	7.34E-07
28	0.40	0.40	449	4869	0.153	49	5.35E+02	1.27E-02	9.93E-07
29	0.40	0.50	395	3189	0.078	37	1.84E+03	1.74E-03	3.23E-07
30	0.25	0.30	450	4000	0.115	42	0	1.30E-02	1.31E-06
31	0.10	0.20	590	2126	0.191	27	0	1.58E-02	9.41E-07
32	0.40	0.40	449	4869	0.153	49	5.67E+01	1.34E-02	1.01E-06

$$[RNH_2] = (1 - 2\theta)\, x, \tag{5}$$

$$\left[RNHCOO^-\right] = \left[RNH_3^+\right] = \theta x, \tag{6}$$

where θ is the CO_2 loading (mol of CO_2/mol of MEA) and x is the MEA molar fraction.

Upon substituting Eqns (5) and (6) back to Eqn (4), the molar fraction of CO_2 dissolved in the MEA solution can be written as

$$\left[CO_2\,(aq)\right] = K'_{CO_2} \frac{\theta^2}{(1 - 2\theta)^2}. \tag{7}$$

By applying Henry's law, the partial pressure of CO_2 can be expressed as

$$p_{CO_2} = K_{CO_2} \frac{\theta^2}{(1 - 2\theta)^2}, \tag{8}$$

where $K_{CO_2} = K'_{CO_2} H^{px}$, and H^{px} is the Henry's constant (kPa). Gabrielsen *et al.*[33] provide an

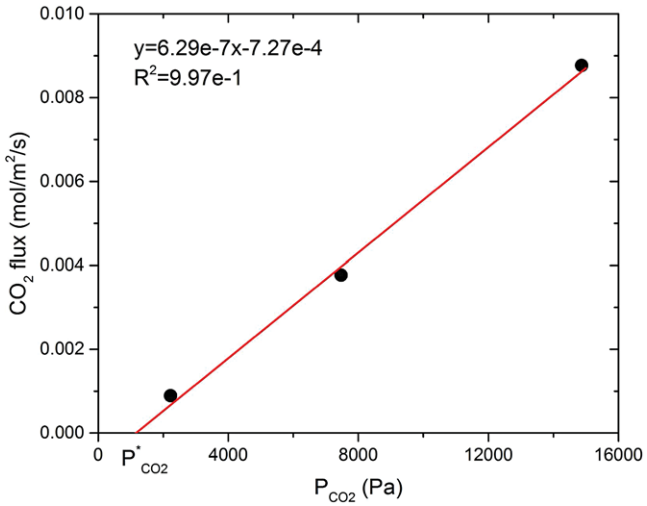

Figure 2. Plot for estimating $P^*_{CO_2}$ for Run No. 6. The x-axis intercept is the approximated value for $P^*_{CO_2}$.

expression for K_{CO_2} as a function of loading and temperature:

$$ln\, K_{CO_2} = A + \frac{B}{T} + C\theta x, \tag{9}$$

where $A = 30.96 \pm 1.86$ and $B = -10584 \pm 670$ denote the standard temperature dependence of the chemical equilibrium constant and $C = -7.187 \pm 4.27$ represents the nonidealities in the system caused by CO_2 loading.

Then, equilibrium aqueous CO_2 concentration dissolved in MEA solution, $c_{CO_2(aq)}$ can be computed as

$$c_{CO_2(aq)} = \frac{p_{CO_2}}{RT}\frac{1}{k}, \tag{10}$$

where k is the dimensionless Henry's constant.

The chemical-reaction-related term in Eqn (3) then can be computed as

$$W_{CO_2} = \mathrm{r}\left(c_{CO_2} - c_{CO_2(aq)}\right) c_{MEA}\alpha_L. \tag{11}$$

Then, the reaction rate constant r (m^3/(mol·s)) in Eqn (11) can be calculated based on a regressed model using the data obtained by Ali:[34]

$$ln\, r = 20.54 - 5612.91/T. \tag{12}$$

By introducing the equilibrium CO_2 concentration, $c_{CO_2(aq)}$, the numerical model can simulate both chemical absorption and desorption of CO_2 in MEA. Also, for non-reactive gas absorption across liquid films, the reaction rate constant r must be set to zero to drop the chemical-reaction-related term W in Eqn (3).

Calculation of overall mass transfer coefficient

Equation (1) is used to calculate the overall mass transfer coefficient for the CO_2/MEA system. Here, the mass transfer flux at the gas-liquid interface consists of two parts. In addition to the physical dissolution of CO_2 in MEA, the chemical absorption of CO_2 in MEA also must be taken into consideration. In Part 1 of this work, the mass transfer flux due to physical dissolution of CO_2 in MEA has been illustrated using N_2O as a surrogate of CO_2. The absorption/desorption of CO_2 stemming from a chemical reaction can be calculated by the conservation law:

$$N = N_1 + N_2 - N_3 - N_4, \tag{13}$$

where N is molar flow rate (mol/(m·s)) per unit depth and N_1 and N_2 represent CO_2 molar flow rate coming in from the gas and solvent inlet, respectively, while N_3 and N_4 represent the CO_2 molar flow rate going out of the solvent and gas outlet, respectively. By calculating the difference between the amount of CO_2 coming in from both the gas and solvent inlets and the amount of CO_2 going out from both the gas and solvent outlets, we can determine the absorbed/desorbed amount of CO_2 inside the WWC due to chemical reaction, which is N in Eqn (13).

Comparison between CFD predictions and correlation results

In the two-film theory,[35] the overall mass transfer coefficient, K_G, can be defined as the harmonic average of the mass transfer coefficient of gas and liquid films:

$$\frac{1}{K_G} = \frac{1}{k_g} + \frac{1}{Ek_L}, \tag{14}$$

where k_g and k_L are the mass transfer coefficients for gas and liquid film, respectively, and E is the enhancement factor that defines the ratio of flux with chemical reactions to those without. Part 1 of this study has introduced the determination of gas and liquid film mass transfer coefficients. The overall enhancement factor is determined using analytical approximations from Dang and Rochelle's work:[36]

$$\frac{1}{E} = \frac{1}{E_l} + \frac{1}{E_{inst}}, \tag{15}$$

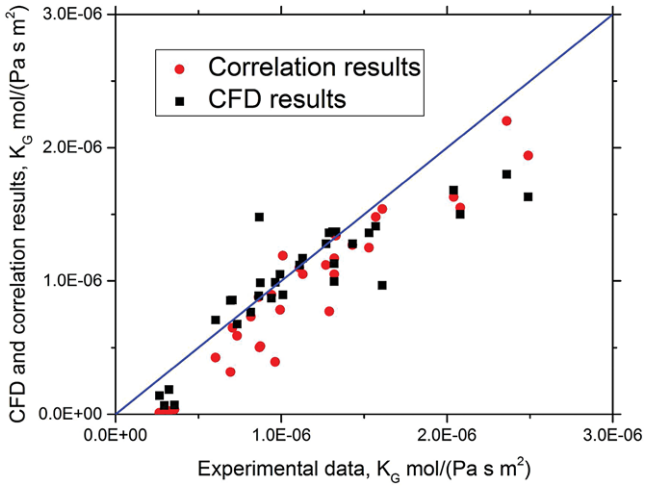

Figure 3. Numerical simulation and correlation results versus experimental data for overall mass transfer coefficient in the CO_2/MEA system. The numerical and correlation results match reasonably well with experimental results.

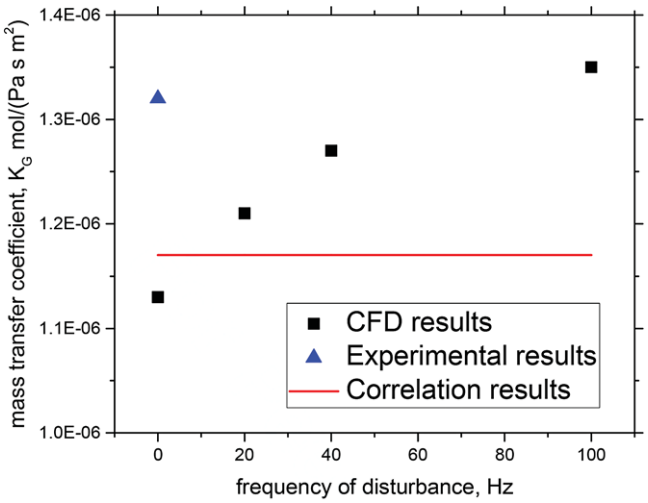

Figure 4. Mass transfer coefficient versus surface wave frequencies for simulation, experimental, and correlation results. The mass transfer coefficient increases with frequencies for simulation results. However, the mass transfer coefficient calculated by correlations is independent of frequencies.

where E_l is the pseudo-first-order enhancement factor and E_{inst} is the instantaneous enhancement factor. Specifically, E_l can be derived by shell balance:

$$E_l = \frac{\sqrt{k_{MEA} C_{MEA,bulk} D_{CO2}}}{k_L}, \qquad (16)$$

where $k_{MEA}(\frac{m^3}{mol \cdot s}) = 0.001 * 10^{10.99-2152/T(K)}$, $C_{MEA,bulk}$ is bulk MEA concentration, and D_{CO2} is the diffusivity of CO_2 in MEA. The estimation of E_{inst} can be expressed as

$$E_{inst} = C_{MEA,total} H^{pc}_{CO2} \frac{\partial\,(loading)}{\partial P^*_{CO2}} \sqrt{\frac{D_{CO2}}{D_{product}}}, \qquad (17)$$

where $C_{MEA,total}$ is total MEA concentration, H^{pc}_{CO2} is the Henry's constant in the unit of m^3/(mol·Pa), and $\frac{D_{CO2}}{D_{product}} \approx 2$, $\frac{\partial(loading)}{\partial P^*_{CO2}}$ is obtained from the vapor-liquid equilibrium model.[36] However, for CO_2 loading less than 0.3, $\frac{\partial(P^*_{CO2})}{\partial loading} \approx 0$.

Figure 3 compares the simulation (highlighted in black squares) and correlations (highlighted in red circles) predicted mass transfer coefficient and experimental measurement results for the CO_2/MEA system. In general, the mass transfer coefficients predicted by numerical simulation and correlations are in good agreement with the corresponding experimental results because all data points distribute around the blue line (slope of 1, meaning 100% match). However, most correlation results predict slightly lower mass transfer coefficients than the experimental measurements. In addition, CFD predictions are better at lower mass transfer, whereas correlation estimations improve at larger mass transfer compared with experimental results. It is evident that the overall mass transfer coefficient in the CO_2/MEA system is almost two orders of magnitude larger than that of the N_2O/MEA system (results are in Part 1 of this series study), which demonstrates that chemical absorption is much larger than physical absorption of CO_2 in MEA solvent.

Similar to Part 1 of this series study, additional CFD simulations for WWC with induced surface waves are run by varying the frequencies of solvent injection rates at the inlet. The solvent inlet velocity is described using a sinusoidal function to generate surface waves:

$$v_s = 0.1768\left[1 + 0.05\sin\left(2\pi f t\right)\right], \qquad (18)$$

where v_s denotes the solvent inlet velocity, t is time, and f represents the controlled frequency. With four frequencies ($f = 0$, 20, 40, and 100) tested, the simulation results (highlighted in black squares) shown in Fig. 4 indicate that the mass transfer coefficient increases with the frequencies, which also is consistent with experimental findings in the literature.[37] However, mass transfer coefficients predicted using correlation show independence on frequencies (highlighted in horizontal line). These results demonstrate that our

Table 2. Inputs to the computer model for the reacting case.

Input	Range/Units
Experimental, $\boldsymbol{x}$:	
Temperature	[25, 60] °C
MEA mass fraction	[0.1, 0.4] g MEA/g total
CO_2 loading in MEA	[0.0, 0.5] mol CO_2/mol MEA
Solvent flow rate	[300, 600] ccm
Gas flow rate	[2000, 6000] sccm
Inlet CO_2 molar concentration	[0.03, 0.20] mol/L
Calibration, $\boldsymbol{t}$:	
(H_{N_2O}) Henry's coefficient	[0.2, 0.9] unitless; converted from "$H_{N_2O,units}$"
(D_{N_2O}) Diffusivity	[5e-10, 5e-08] m^2/s
(k_2) Rate Constant	[0, 70] $m^3/(mol \cdot s)$

physical-based numerical model has the capability to predict the effect of flow instabilities on overall mass transfer coefficients of the WWC under some extreme flow conditions, which correlations typically do not cover.

Model calibration and uncertainty quantification analysis

The method used to obtain a statistical design for the experimental reacting data is similar to that of the non-reacting data, and Table 2 lists the inputs for computer model for reactive cases. For this scenario, a set of 32 experiments are planned in such a way that the $\boldsymbol{x}$-space (controllable inputs) would be 'covered' by 29 points, and 3 of those points would be replicated to better estimate true experimental uncertainty. As for the simulations, three batches result in a total of 323 runs. In the first batch, for each experimental run, the corresponding numerical simulations employ the same controlled operating parameters but with three different values for each of the following quantities: Henry's constant, gas diffusivity in solvent, and CO_2 reaction rate constant. Five numerical testing cases are designed for each experimental run (No. 2–29), while a total of 27 numerical testing cases are designed for experimental run No. 1. The second batch is constructed in a similar style, such that there are 29 sets consisting of two to three runs that differ only in settings for the calibration inputs. The third batch (having 74 runs) is designed specifically to aid in the calibration of the reaction rate constant. The controlled parameters in the numerical model are the same as those used in experimental run No. 1 but with two different operating temperatures: 42°C and 30°C, respectively.

The experimental and simulated data are combined using a Bayesian calibration routine.[38] This algorithm requires prior distributions on the statistical parameters of interest (in this case, the coefficients in the functional forms of Henry's coefficient, diffusivity, and the reaction rate constant). Parametric distributions are fit to the posteriors from the non-reacting results and used as the priors in the present analysis. This can be done because the Stokes-Einstein equations given in Table 3 relate the Henry's coefficient (or diffusivity) for N_2O to that of CO_2 via a ratio. Two more parameters have been added to characterize the rate constant (c_8, c_9). The priors on these are uniform on the hyperrectangle $[15, 25] \times [3500, 7500]$, subject to the constraint that k_2 at the highest temperature could not be smaller than 10 or greater than 70.

Table 3. Default relationships for the reacting scenario.

Relationship	Reference/Notes
$H_{CO_2,units} = H_{N_2O,units} \cdot (H_{CO_2,H_2O}/H_{N_2O,H_2O})$	Li and Lai (1995)[28] Eqn (1)
$H_{CO_2,H_2O} = \exp(145.369 - 8172.355/T - 19.303 \cdot \ln T)$	Penttila *et al.* (2011)[39] Eqn (2)
$H_{N_2O,H_2O} = \exp(158.245 - 9048.596/T - 20.860 \cdot \ln T - 0.00252 \cdot T)$	Eqn (3) with Table 1
$D_{CO_2} = D_{N_2O} \cdot (D_{CO_2,H_2O}/D_{N_2O,H_2O})$	Li and Lai (1995)[28] Eqn (2)
$D_{CO_2,H_2O} = (2.35e\text{-}06) \cdot \exp(-2119/T)\ m^2/s$	Eqn (6)
$D_{N_2O,H_2O} = (5.07e\text{-}06) \cdot \exp(-2371/T)\ m^2/s$	Eqn (5)
Rate Constant $k_2 = \exp(c_8 - c_9/T)\ m^3/(mol \cdot s)$	Ali (2005)[34]
$c_8 = 20.54396$	Regressed from data in Table 1
$c_9 = 5612.91378$ K	

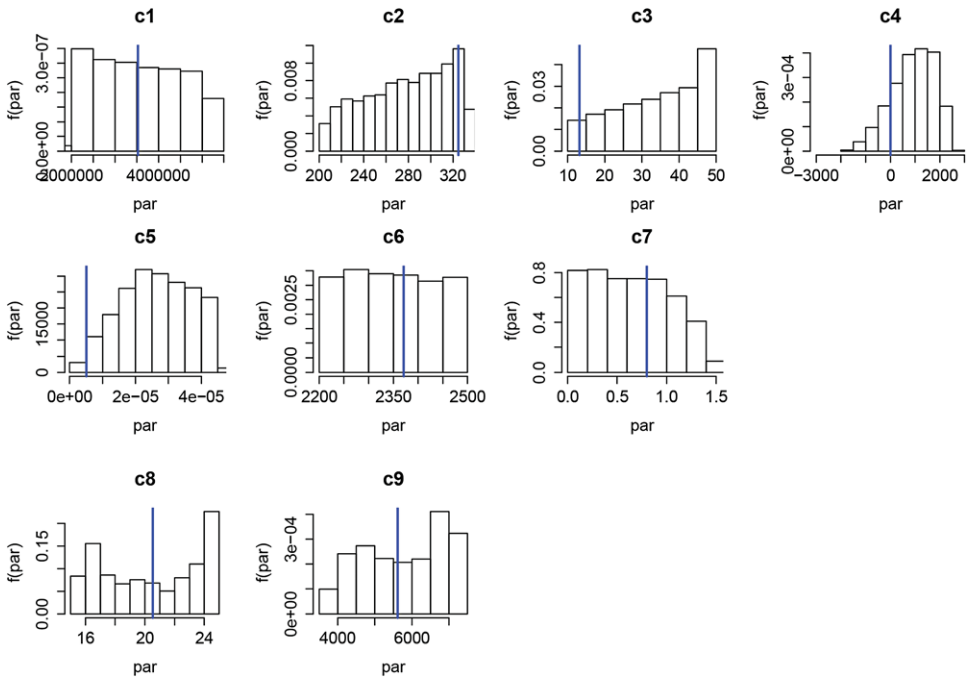

Figure 5. Estimated marginal posterior distributions for the calibration parameters of the reacting scenario. The blue line segments are the point estimates found in the literature. The definition of c1–c7 can be found in Part 1 of this work.[29] The definitions of c8 and c9 are listed in Table 3.

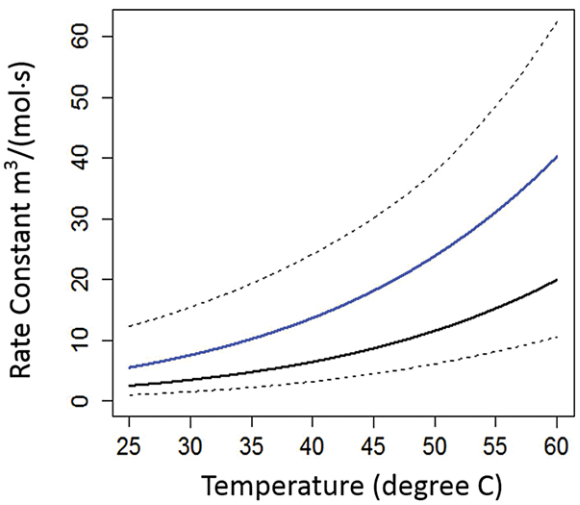

Figure 6. Uncertainty in the rate constant as a function of temperature. The blue curve is derived from the literature, while the black curve is the median prediction. The dashed lines form pointwise 90% intervals.

To achieve convergence, the calibration routine is run for a total of 110,000 iterations, and the results can be found in Fig. 5 and Fig. 6. It can be seen that the posteriors for c_1 – c_7 (parameterizing Henry's coefficient and diffusivity) after this calibration are not qualitatively different from the posteriors after the non-reacting calibration. That is to say, there is not much information about these quantities after combining the experimental and simulated reacting data. The data seemingly could only inform the parameterization of the reaction rate constant, but this may be reasonable.

Conclusion

A series of WWC experiments consisting of 32 runs generated using statistical design of experiment strategy with varying conditions have been conducted to assist the study of reactive mass transport of CO_2 into MEA solvent. A comprehensive numerical model has been developed to investigate gas absorption/desorption for reactive CO_2/MEA system using a custom-built CFD software package, OpenFOAM. Traditional/empirical correlations are also implemented to help distinguish the wider applicability of the CFD model. In general, both numerical and correlation predictions have good agreement with experimental results in the laminar flow regime. However, under some extreme flow

conditions, for example wavy falling films with controlled frequencies, the physics-based numerical model can naturally account for the dependence of mass transfer coefficient on frequencies, whereas correlations normally cannot capture these flow instabilities on mass transfer. It has been found that chemical absorption is the major contribution to CO_2 capture compared to physical absorption. We have demonstrated that the Bayesian calibration methodology can be used to validate models, as well as quantify and propagate parametric uncertainties. From here, it would be possible, for example, to pass the samples from the second-stage posteriors through a model of an upscaled system to get prediction intervals.

Acknowledgements

Pacific Northwest National Laboratory is operated by Battelle for the US Department of Energy (DOE) under Contract No. DE-AC05-76RL01830. This work was funded by the DOE Office of Fossil Energy's Carbon Capture Simulation Initiative through the National Energy Technology Laboratory.

Disclaimer

References

1. Xu Z, Lai C, Marcy PW, Dietiker J-F, Li T, Sarkar A *et al.*, Predicting the performance uncertainty of a 1-MW pilot-scale carbon capture system after hierarchical laboratory-scale calibration and validation. *Powder Technology* **312**:58–66 (2017).
2. Lai C, Xu Z, Li T, Lee A, Dietiker J-F, Lane W *et al.*, Effects of heat exchanger tubes on hydrodynamics and CO_2 capture of a sorbent-based fluidized bed reactor. *Powder Technology* **322**(Supplement C):202–213 (2017).
3. Lai C, Xu Z, Pan W, Sun X, Storlie C, Marcy P *et al.*, Hierarchical calibration and validation of computational fluid dynamics models for solid sorbent-based carbon capture. *Powder Technology* **288**:388–406 (2016).
4. Xu Z, Sun X, Khaleel MA, A generalized kinetic model for heterogeneous gas-solid reactions. *The Journal of Chemical Physics* **137**(7):074702 (2012).
5. Singh RK, Galvin JE, Sun X, Hydrodynamics of the rivulet flow over corrugated sheet used in structured packings. *International Journal of Greenhouse Gas Control* **64**(Supplement C):87–98 (2017).
6. Singh RK, Galvin JE, Sun X, Three-dimensional simulation of rivulet and film flows over an inclined plate: Effects of solvent properties and contact angle. *Chemical Engineering Science* **142**:244–257 (2016).
7. Astarita G, Carbon dioxide absorption in aqueous monoethanolamine solutions. *Chem Eng Sci* **16**(3):202–207 (1961).
8. Danckwerts PV and Sharma MM, Absorption of Carbon dioxide into solutions of alkalis and amines (with some notes on hydrogen sulphide and carbonyl sulphide). *Trans Inst Chem Eng* **44**(8):C244–C244 (1966).
9. Yu C-H, Huang C-H and Tan C-S, A review of CO_2 capture by absorption and adsorption. *Aerosol Air Qual Res* **12**(5):745–769 (2012).
10. Blauwhoff PMM, Versteeg GF and Van Swaaij WPM, A study on the reaction between CO_2 and alkanolamines in aqueous solutions. *Chem Eng Sci* **39**(2):207–225 (1984).
11. Crooks JE and Donnellan JP, Kinetics and mechanism of the reaction between carbon dioxide and amines in aqueous solution. *J Chem Soc Perkin Trans* (4):331–333 (1989).
12. Danckwerts PV, The reaction of CO_2 with ethanolamines. *Chem Eng Sci* **34**(4):443–446 (1979).
13. Donaldson TL and Nguyen YN, Carbon-Dioxide reaction-kinetics and transport in aqueous amine membranes. *Ind Eng Chem Fund* **19**(3):260–266 (1980).
14. Vaidya PD and Kenig EY, CO_2-alkanolamine reaction kinetics: A review of recent studies. *Chem Eng Technol* **30**(11):1467–1474 (2007).
15. Versteeg GF and van Swaaij WPM, On the kinetics between CO_2 and alkanolamines both in aqueous and non-aqueous solutions—I. Primary and secondary amines. *Chem Eng Sci* **43**(3):573–585 (1988).
16. Hikita H, Asai S, Ishikawa H and Honda M, Kinetics of reactions of carbon-dioxide with monoethanolamine, diethanolamine and triethanolamine by a rapid mixing method. *Chem Eng J Biochem Eng J* **13**(1):7–12 (1977).
17. Laddha SS and Danckwerts PV, Reaction of CO_2 with ethanolamines - kinetics from gas-absorption. *Chem Eng Sci* **36**(3):479–482 (1981).
18. Danckwerts PV. *Gas–Liquid Reactions*. McGraw-Hill Book Company, New York (1970).
19. Astarita G, Savage DW and Bistro A, *Gas Treating with Chemical Solvents*. John Wiley & Sons, Inc., New York; 1983.
20. Bishnoi S and Rochelle GT, Absorption of carbon dioxide into aqueous piperazine: reaction kinetics, mass transfer and solubility. *Chem Eng Sci* **55**(22):5531–5543 (2000).

21. Jou FY, Mather AE and Otto FD, The solubility of CO_2 in a 30-mass-percent monoethanolamine solution. *Can J Chem Eng* **73**(1):140–147 (1995).
22. Lee J, Otto FD and Mather AE, The solubility of H_2S and CO_2 in aqueous monoethanolamine solutions. *Can J Chem Eng* **52**(6):803–805 (1974).
23. Lee JI, Otto FD and Mather AE, Equilibrium between carbon dioxide and aqueous monoethanolamine solutions. *J Appl Chem Biotechnol* **26**(1):541–549 (1976).
24. Park MK and Sandall OC, Solubility of carbon dioxide and nitrous oxide in 50 mass % methyldiethanolamine. *Journal of Chemical and Engineering Data* **46**(1):166–168 (2001).
25. Shen KP and Li MH, Solubility of carbon dioxide in aqueous mixtures of monoethanolamine with methyldiethanolamine. *J Chem Eng Data* **37**(1):96–100 (1992).
26. Versteeg GF and Vanswaaij WPM, Solubility and diffusivity of acid gases (CO_2, N_2O) in Aqueous alkanolamine solutions. *J Chem Eng Data* **33**(1):29–34 (1988).
27. Ying JR, Eimer DA and Yi WJ, Measurements and correlation of physical solubility of carbon dioxide in (monoethanolamine plus water) by a modified technique. *Ind Eng Chem Res* **51**(19):6958–6966 (2012).
28. Li MH and Lai MD, Solubility and diffusivity of N_2O and CO_2 in (Monoethanolamine Plus N-Methyldiethanolamine Plus Water) and in (Monoethanolamine Plus 2-Amino-2-Methyl-1-Propanol Plus Water). *J Chem Eng Data* **40**(2):486–492 (1995).
29. Wang C, Xu Z, Lai C, Whyatt G, Marcy P and Sun X, Hierarchical calibration and validation for modeling bench-scale solvent-based carbon capture. Part 1: Non-reactive physical mass transfer across the wetted wall column. *Greenh Gas Sci Technol* 2017 (in press).
30. Aronu UE, Gondal S, Hessen ET, Haug-Warberg T, Hartono A, Hoff KA *et al*., Solubility of CO_2 in 15, 30, 45 and 60 mass% MEA from 40 to 120 degrees C and model representation using the extended UNIQUAC framework. *Chem Eng Sci* **66**(24):6393–6406 (2011).
31. Haroun Y, Legendre D and Raynal L, Direct numerical simulation of reactive absorption in gas-liquid flow on structured packing using interface capturing method. *Chem Eng Sci* **65**(1):351–356 (2010).
32. Haroun Y, Legendre D and Raynal L, Volume of fluid method for interfacial reactive mass transfer: Application to stable liquid film. *Chem Eng Sci* **65**(10):2896–2909 (2010).
33. Gabrielsen J, Michelsen ML, Stenby EH and Kontogeorgis GM, A model for estimating CO_2 solubility in aqueous alkanolamines. *Ind Eng Chem Res* **44**(9):3348–3354 (2005).
34. Ali SH, Kinetics of the reaction of carbon dioxide with blends of amines in aqueous media using the stopped-flow technique. *Int J Chem Kin* **37**(7):391–405 (2005).
35. Whitman WG, Preliminary experimental confirmation of the two-film theory of gas absorption. *Chem Metall Eng* **29**:146–149 (1923).
36. Dang H and Rochelle GT, CO_2 absorption rate and solubility in monoethanolamine/piperazine/water. *Separation science and technology* **38**(2):337–357 (2003).
37. Yoshimura PN, Nosoko T and Nagata T, Enhancement of mass transfer into a falling laminar liquid film by twig-dimensional surface waves – Some experimental observations and modeling. *Chem Eng Sci* **51**(8):1231–1240 (1996).
38. Kennedy MC and O'Hagan A, Bayesian calibration of computer models. *J R Stat Soc B* **63**:425–450 (2001).
39. Penttila A, Dell'Era C, Uusi-Kyyny P and Alopaeus V, The Henry's law constant of N2O and CO2 in aqueous binary and ternary amine solutions (MEA, DEA, DIPA, MDEA, and AMP). *Fluid Phase Equilibria* **311**:59–66 (2011).

Chao Wang

Dr Chao Wang received his PhD from Mechanical and Materials Engineering Department at Wright State University in 2013. Currently, he is a staff scientist in Computational Engineering Group at Pacific Northwest National Laboratory. His research interest includes computational fluid dynamics, multi-phase flow, discrete element method, finite element method, uncertainty quantification, reduced order model (ROM), and integrated computational materials engineering (ICME).

Zhijie Xu

Dr Zhijie Xu is a staff scientist in Computational Mathematics Group at Pacific Northwest National Laboratory. Dr Zhijie Xu's current work involves computational modeling of multiphase reactive flow with applications to carbon capture and sequestration. He holds PhD in Mechanical Engineering from Rensselaer Polytechnic Institute, NY. His PhD research involved the development of large-scale parallel simulation tools for multiscale (atomistic to continuum) modeling of materials. Dr Xu has published more than 70 peer-reviewed journal articles and book chapters.

Kevin Lai

Dr Kevin Lai obtained his PhD from University of Michigan. He is currently working at Oak Ridge National Laboratory. His research interest includes software and algorithm development, numerical analysis and multi-physics modeling.

Greg Whyatt

Greg Whyatt holds an MS degree in chemical engineering from Washington State University and is a licensed professional engineer in the state of Washington. Since joining PNNL in 1987, Greg has been involved in a wide range of projects. Greg is inventor on 18 granted US patents.

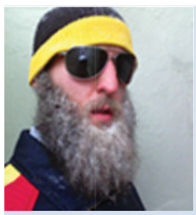

Peter W. Marcy

Peter W. Marcy is a scientist in the Statistical Sciences Group (CCS-6) at Los Alamos National Laboratory. He has broad experience in Bayesian statistics and UQ with application areas including environmental, chemical, nuclear, and petroleum engineering, high-energy physics, and materials science.

Xin Sun

Dr Xin Sun is the Director for the Energy and Transportation Science Division at Oak Ridge National Laboratory (ORNL). Her research expertise lies in the areas of computational materials and applied mechanics, and her strength is in applying the mechanics and materials fundamentals in solving challenging energy materials problems ranging from multi-physics carbon capture device-scale simulations to lightweight materials manufacturing processes including forming, joining and non-destructive evaluations. Prior to joining ORNL, Dr Sun was a Laboratory Fellow at Pacific Northwest National Laboratory in Richland, Washington. Dr Sun is a well-recognized expert in Integrated Computational Materials Engineering (ICME) for lightweight energy materials, and has published more than 170 peer-reviewed journal articles and 10 books/book chapters. Dr Sun has earned many recognitions for her technical accomplishments, with the most notables including the R&D 100 Award (2016), the University of Michigan Alumni Society Merit Award (2009), and PNNL Laboratory Director's Award for Exceptional Engineering Achievement (2008).

